Nanoscale

Accepted Manuscript

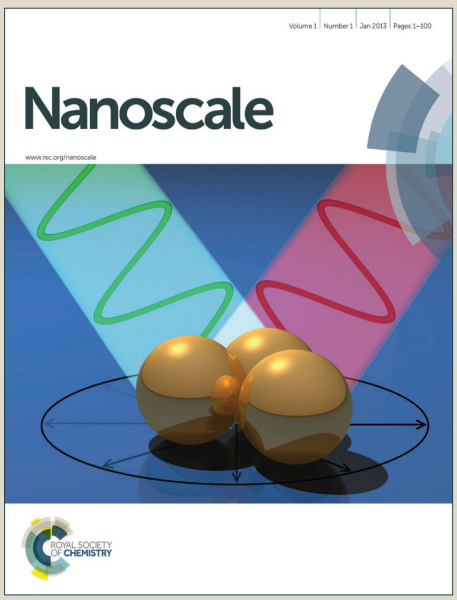

ROYAL SOCIETY OF CHEMISTRY

www.rsc.org/nanoscale

Nanoscale

RSCPublishing

COMMUNICATION

Highly Efficient and Low Voltage Silver Nanowire-Based OLEDs employing n-Type Hole Injection Layer

Cite this: DOI: 10.1039/x0xx00000x

Hyungjin Lee,[a] Donghwa Lee,[a] Yumi Ahn,[a] Eun-Woo Lee,[b] Lee Soon Park[c] and Youngu Lee*[a]

Received 00th January 2014,
Accepted 00th January 2014

DOI: 10.1039/x0xx00000x

www.rsc.org/

Highly flexible and efficient silver nanowire-based organic light-emitting diodes (OLEDs) have been successfully fabricated by employing n-type hole injection layer (HIL). The silver nanowire-based OLEDs without light outcoupling structures exhibited excellent device characteristics such as extremely low turn-on voltage (3.6 V) and high current and power efficiencies (44.5 cdA^{-1} and 35.8 lmW^{-1}). In addition, flexible OLEDs with the silver nanowire transparent conducting electrode (TCE) and n-type HIL fabricated onto plastic substrates showed remarkable mechanical flexibility as well as device performance.

Flexible organic light-emitting diode panels have been considered as essential elements of next generation displays due to excellent mechanical bend ability, low power consumption, superb color gamut, wide viewing angle, fast response time, and design flexibility.[1-4] To fabricate flexible OLEDs, the first thing we have to do is to get rid of a vacuum-deposited ITO TCE as well as a rigid glass substrate. In conventional OLED panels, ITO has been utilized as an anode material since it possesses excellent physical properties such as high optical transmittance in visible region and low sheet resistance.[5-11] However, it has critical drawbacks such as brittleness, high refractive index, and high processing temperature, which are not suitable for flexible applications.[12-17] For instance, when mechanical stress is applied onto OLEDs, the efficiency and brightness of the OLEDs can be greatly diminished due to the fracture of ITO.[15-17] Therefore, it is necessary to develop alternative TCEs which are better suited for next generation flexible OLEDs.

Recently, silver nanowires (AgNWs) TCE has been considered as one of the most promising materials to replace ITO for flexible optoelectronic devices such as OLEDs, touch screen panels (TSPs), and solar cells thanks to its excellent electrical, optical, and mechanical properties.[14-25] However, the inherent surface roughness and low work function value of the AgNWs TCE are considered as drawbacks against fabrication of reliable and high performance OLEDs. Since the AgNWs TCE is based on a random network of the AgNWs with 20~100 nm in diameter, the overlapping AgNWs might lead to protrusions or spikes causing electrical shorts in OLEDs.[17-21] Thus, for improvement of fabrication yield of OLEDs based on the AgNWs TCE, the protrusions and local spikes on the AgNWs surface need to be completely covered by the hole injection layer. In addition, compared to ITO, the AgNWs TCE possesses low work function value, which is not closely matched with conventional amine-type HIL materials, leading to high hole injection barriers. Recently, PEDOT:PSS has been utilized as HIL for AgNWs based OLEDs. However, they showed very high turn-on voltage and poor device performances due to high hole injection barrier and energy level mismatch.[16, 25, 26] Therefore, it is necessary to develop suitable HIL materials for the AgNWs TCE in order to simultaneously achieve smooth surface morphology and low hole injection barrier for high-performance OLEDs.

Here, we report a combination system of the AgNWs TCE and n-type HIL for extremely flexible and high-performance phosphorescent OLEDs (PHOLEDs). We demonstrate a new approach to obtain a smooth surface morphology and decrease hole injection barrier by using 1,4,5,8,9,11-hexaazatriphenylene-hexacarbonitrile (HAT-CN) as a hole injection layer between the

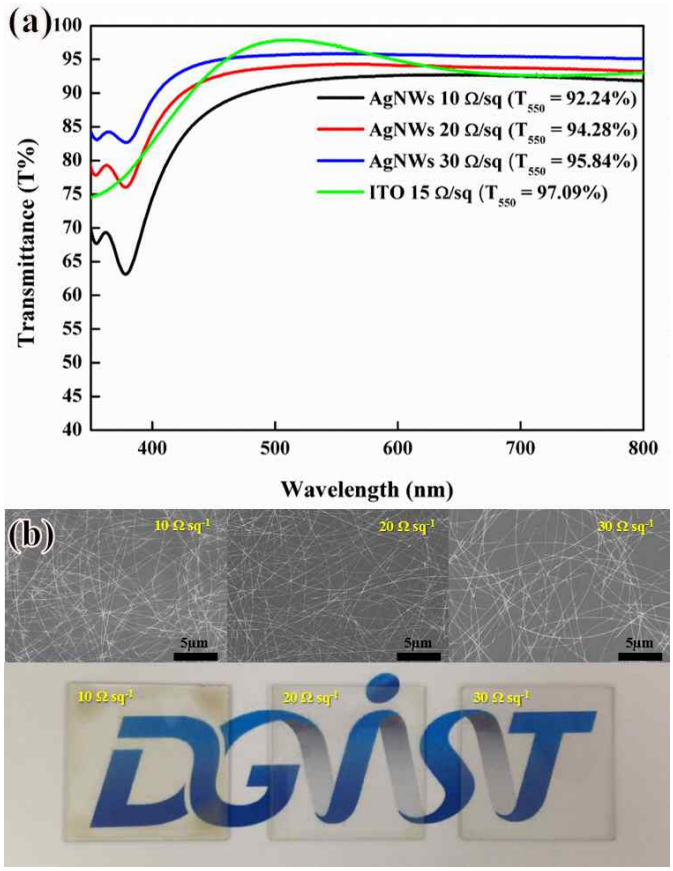

Fig. 1 (a) UV/Vis spectra of AgNWs TCEs with different sheet resistance values and (b) The SEM images and pictures of AgNWs TCEs with different sheet resistance values on glass substrate.

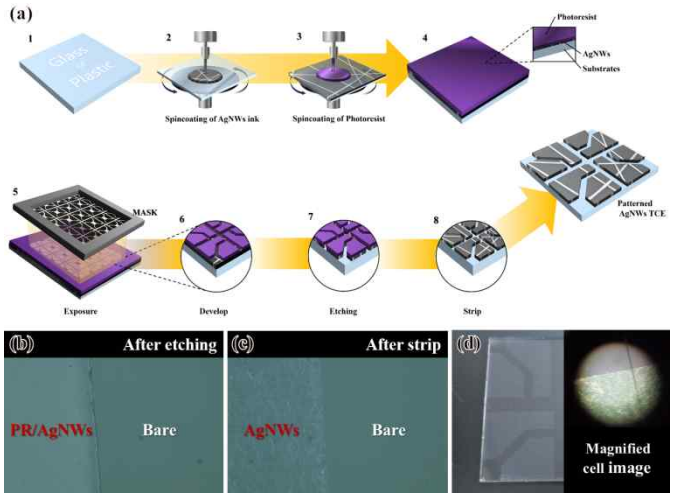

Fig. 2 (a) Schematic illustration of a photolithographic process for patterned AgNWs TCE. Magnified optical images of AgNWs pattern (b) after etching process and (c) after strip process. (d) A photograph of patterned AgNWs TCE for the fabrication of OLEDs. The inset shows a magnified image of AgNWs pattern.

AgNWs TCE and hole transporting layer (HTL). HAT-CN is a n-type discotic organic semiconductor, which possesses a deep lowest occupied molecular orbital (LUMO) energy level (~5.5 eV).[27] It has been reported that HAT-CN successfully acts as a HIL material in OLEDs because the LUMO energy level of HAT-CN facilitates efficient hole injection and transport from an anode to a HTL.[28-30] Therefore, we employed a thick HAT-CN layer (over 150 nm) as a HIL to obtain extremely reliable and high-performance PHOLEDs with AgNWs TCE. The fabricated PHOLEDs without light outcoupling structures exhibited excellent device performances such as very low turn-on voltage (3.6 V) and exceedingly high current and power efficiencies (44.5 cdA^{-1} and 35.8 lmW^{-1}). In addition, flexible PHOLEDs with the AgNWs TCE and HAT-CN fabricated onto plastic substrates showed remarkable device performances and mechanical flexibility. It was found that employing HAT-CN as a HIL between AgNWs TCE and α-NPB could decrease the hole injection barrier, leading to significant improvement in current and power efficiencies of PHOLEDs.

The AgNWs TCE was prepared by spin-coating a AgNWs (average diameter and length of 20~40 nm and 10~20 μm, respectively) ink on a substrate such as a glass or plastic to investigate the optical, electrical, and mechanical properties. We treated the substrate with UV/ozone to make hydrophilic surfaces. Then, the AgNWs ink was spin-coated at various spin coating rates on the pre-cleaned substrate and then dried at 120 ºC for 5 min. We measured the optical transmittance and sheet resistance of the AgNWs TCE using UV/Vis spectroscopy and non-contact sheet resistance measurement system (Fig. 1). The optical transmittance and sheet resistance of the AgNWs TCE were 92.2% at 550 nm and 10 ± 0.5 Ω/sq, indicating that the AgNWs TCE exhibited superior optical transparency and electrical conductivity comparable to conventional ITO TCE. The mechanical flexibility of the AgNWs TCE was investigated as a function of wrapping cycles. A flexible AgNWs TCE was prepared on a polyethylene naphthalate (PEN) substrate using the spin-coating of the AgNWs ink. In this test, a piece of the AgNWs TCE/PEN was rolled around bending radius of 7.5 mm, subsequently unrolled at a speed of 30 mm/sec, and the sheet resistance was compared to its initial value.

The sheet resistance of the AgNWs TCE/PEN remained unchanged after more than 10,000 wrapping cycles, verifying that the AgNWs TCE/PEN possesses an excellent mechanical flexibility (Fig. S1). For fabrication of OLED devices with the AgNWs TCE, the AgNWs TCE was successfully patterned on a glass substrate by using a photolithographic process. Fig. 2a shows a schematic illustration of a photolithographic process for AgNWs TCE. Magnified optical images of each process steps prove successful photolithographic process with uniform pattern as shown in Fig. 2b~d. Then, we fabricated a series of small-molecule phosphorescent OLEDs (PHOLEDs) with the patterned AgNWs TCE and different hole injection materials such as HAT-CN or N,N'-diphenyl-N,N'-bis[4-(phenyl-m-tolyl-amino)phenyl]-biphenyl-4,4'-diamine (DNTPD). We also fabricated ITO based PHOLEDs with the different thickness of HAT-CN as reference devices. The device structure and the chemical structure of the materials used for the PHOLEDs are shown in Fig. 3a. Each thickness of HAT-CN and DNTPD as the hole injection layer was systematically varied with the fixed thickness of other layers. All organic layers were successfully deposited on the patterned TCEs at a base pressure of < 3 x 10^{-7} Torr without breaking the

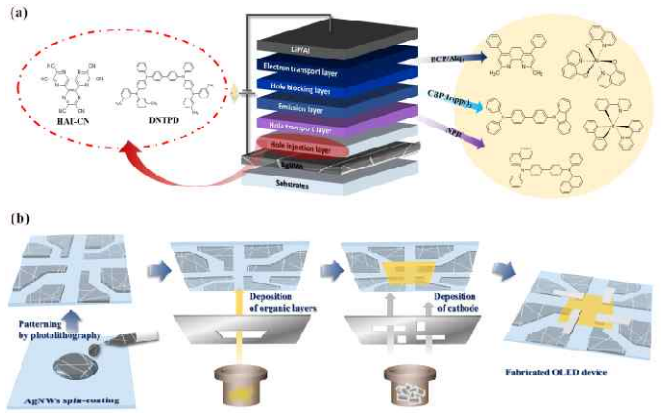

Fig. 3 Schematic illustrations of device structure and fabrication process for PHOLEDs with AgNWs TCE. (a) Device structure and chemical structure of the materials used for the PHOLEDs. (b) A schematic illustration of the fabrication for PHOLEDs with AgNWs TCE.

vacuum in a cluster type OLED manufacturing system. Fig. 3b shows a schematic illustration of fabrication process for PHOLED devices with the AgNWs TCE. Six different green PHOLEDs prepared for evaluating the effect of hole injection layer on each TCE in this study were as follows:

Device A: AgNWs TCE/HAT-CN (150 nm)/α-NPB (40 nm)/CBP:Ir(ppy)$_3$ (10%, 20 nm)/BCP (20 nm)/Alq$_3$ (40 nm)/LiF/Al

Device B: AgNWs TCE/HAT-CN (200 nm)/α-NPB (40 nm)/CBP:Ir(ppy)$_3$ (10%, 20 nm)/BCP (20 nm)/Alq$_3$ (40 nm)/LiF/Al

Device C: AgNWs TCE/DNTPD (150 nm)/α-NPB (40 nm)/CBP:Ir(ppy)$_3$ (10%, 20 nm)/BCP (20 nm)/Alq$_3$ (40 nm)/LiF/Al

Device D: AgNWs TCE/DNTPD (200 nm)/α-NPB (40 nm)/CBP:Ir(ppy)$_3$ (10%, 20 nm)/BCP (20 nm)/Alq$_3$ (40 nm)/LiF/Al

Device E: ITO TCE/HAT-CN (150 nm)/α-NPB (40 nm)/CBP:Ir(ppy)$_3$ (10%, 20 nm)/BCP (20 nm)/Alq$_3$ (40 nm)/LiF/Al

Device F: ITO TCE/HAT-CN (200 nm)/α-NPB (40 nm)/CBP:Ir(ppy)$_3$ (10%, 20 nm)/BCP (20 nm)/Alq$_3$ (40 nm)/LiF/Al

It is noteworthy that at least 150-nm-thick film of HAT-CN or DNTPD is required in order to completely planarize the rough surface and remove local spikes on the AgNWs TCE (Fig. S2). Therefore, we employed a thick HIL film over 150 nm to fabricate reliable PHOLED devices.

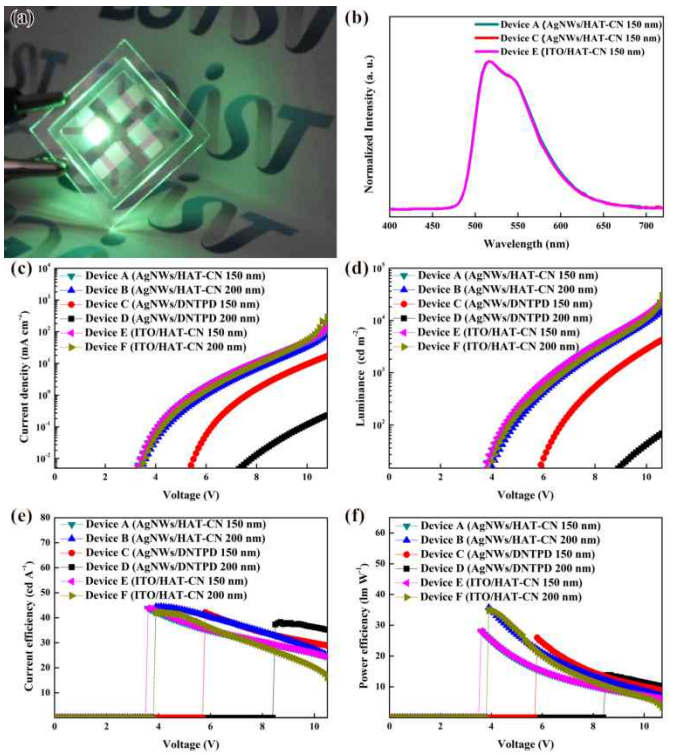

Fig. 4 Device performance of green PHOLEDs with AgNWs and ITO TCE. (a) A picture of an encapsulated green PHOLED on the patterned AgNWs TCE. (b) The electroluminescence spectra of PHOLED Devices with HAT-CN and DNTPD HILs (150 nm) on each patterned TCE. Device characteristics such as (c) current density (d) luminance (e) current efficiency, and (f) power efficiency of green PHOLEDs with different thickness of the HAT-CN and DNTPD HILs on each patterned TCE.

All the PHOLEDs with 150-nm-thick HIL film can operate properly without any electrical shorts as shown in Fig. 4a. The electroluminescence (EL) spectra of the PHOLEDs with HAT-CN or DNTPD HILs were shown in Fig. 4b. All the PHOLEDs exhibited typical green electroluminescence from Ir(ppy)$_3$ with a Commission Internationale de l'Eclairage (CIE) coordinate (0.32, 0.61). To evaluate the effect of the AgNWs TCE and HAT-CN HIL on devices performances of PHOLEDs, we measured the current density − voltage − luminance (J − V − L) characteristics.

Table 1 Device characteristics of PHOLEDs with different thickness of HAT-CN and DNTPD HILs on the AgNWs TCE.

Device	TCE	HIL		Turn-on voltage	Efficiencies		Luminance	
		Material	Thickness		Max CE	Max PE	Voltage at Max Luminance	Max Luminance
			[nm]	[V]	[cd/A]	[lm/W]	[V]	[cd/m^2]
Device A	AGNWs	HAT-CN	150	3.6	43.8	28.1	11.1	45170
Device B	AGNWs	HAT-CN	200	3.9	44.5	35.8	11.1	39020
Device C	AGNWs	DNTPD	150	5.8	42.2	26.0	13.2	47550
Device D	AGNWs	DNTPD	200	8.5	37.9	13.8	-	-
Device E	ITO	HAT-CN	150	3.6	43.8	28.1	11.0	47830
Device F	ITO	HAT-CN	200	3.9	42.0	35.0	10.7	54270

(CE = current efficiency, PE = power efficiency)

Fig. 4c ~ f present current density (J), luminance (L), current efficiency (cdA^{-1}), and power efficiency (lmW^{-1}) of the fabricated green PHOLEDs with different thickness of the HAT-CN and DNTPD HILs on the AgNWs and ITO TCEs. Table 1 summarize the device characteristics of the fabricated PHOLEDs. As shown in Fig. 4c, The J-V characteristics of the PHOLEDs with HAT-CN on the AgNWs TCE (device A and B) clearly show the remarkable improvement in hole injection properties compared to the control devices with DNTPD (device C and D). The J- V curve of the PHOLEDs with HAT-CN was shifted towards lower voltage of about 2 ~ 5 V as compared to the control devices with DNTPD. For instance, the device A showed very low turn-on voltages of 3.6 V. To the best of our knowledge, this is the lowest turn-on voltage achieved in AgNWs TCE based OLEDs (Table S1). In addition, the device A achieved high luminance over 45,000 cdm^{-2} as shown in Fig. 4d (Movie S1). Even though the thickness of HAT-CN increased up to 200 nm, the turn-on and operating voltage almost unchanged (3.9 V). On the contrary, the turn-on voltages for device C and D with DNTPD HIL were 5.8 V and 8.9 V, respectively. In addition, the current density of PHOLEDs with HAT-CN (device A and B) was much higher than the control devices with DNTPD (device C and D). These results clearly verify that the PHOLEDs with the AgNWs TCE and HAT-CN showed extremely low turn-on and operating voltage due to efficient hole injection from AgNWs to HAT-CN and charge transport through HAT-CN. The current and power efficiency characteristics of fabricated PHOLEDs are shown in Fig. 4e and f. Device A and B showed extremely high maximum current and power efficiencies of 43.8 cdA^{-1}/28.1 lmW^{-1} and 44.5 cdA^{-1}/35.8 lmW^{-1}, respectively. These results clearly indicate that the device performances of the AgNWs based PHOLEDs are comparable to those of ITO based device E (43.8 cdA^{-1}/28.1 lmW^{-1}) and F (43.8 cdA^{-1}/28.1 lmW^{-1}) with the same device configurations. The remarkably high power efficiency is attributed to the very low operating voltage of PHOLEDs with HAT-CN HIL. External quantum efficiency (EQE) was 14.8% and 15.0% for the device A and B, respectively (Fig. S3). It is noteworthy that it is the highest efficiencies achieved in AgNWs TCE based OLEDs without light outcoupling structures (Table S1). These results demonstrate that the current and power efficiencies of the PHOLEDs with HAT-CN (device A and B) were not affected by the thickness of HAT-CN, which is attributed to efficient hole transport capability of HAT-CN. On the other hand, for the control device with DNTPD HIL, the maximum current and power efficiencies were 42.2 cdA^{-1} and 26.0 lmW^{-1} for the device C and 37.9 cdA^{-1} and 13.8 lmW^{-1} for the device D, indicating that a thicker DNTPD layer increased operating voltage significantly, leading to a sharp decrease of power efficiency. To confirm how HAT-CN is deposited onto the AgNWs TCE, the surface morphology was investigated using a scanning electron microscopy (SEM) and atomic force microscopy (AFM) as shown in Fig. S4 and S5. The surface roughness is mainly determined by the overlap of nanowires and binder concentration. The improvement in microscopic coating quality can be achieved with proper thickness of the HAT-CN. The rough surface of the AgNWs TCE might be planarized by varying the thickness of the HAT-CN. To evaluate the effect of thickness of HAT-CN on the surface morphology, four different films were used: (1) AgNWs/HAT-CN (50 nm), (2) AgNWs/HAT-CN (100 nm), (3) AgNWs/HAT-CN (150 nm), and (4) AgNWs/HAT-CN (200 nm). As shown in Fig. S4, when HAT-CN was deposited onto the AgNWs TCE less than 150 nm, it was still observed that the overlapping AgNWs and local spikes were on the AgNWs surface, resulting in electrical shorts in the devices. However, when 150-nm-thick film of HAT-CN was deposited onto the AgNWs TCE, sufficient planarization was achieved, leading to no electrical shorts observed in the PHOLEDs. In particular, local spikes on the AgNWs surface causing electrical shorts in OLEDs were completely covered. As shown in Fig. S5, The root-mean-square roughness (R_{rms}) values of the AgNWs/HAT-CN films decreased from 19.48 nm to 9.62 nm significantly as the thickness of HAT-CN layer increased from 50 nm to 200 nm. These results clearly verify that at least 150-nm-thick film of HAT-CN is required in order to completely planarize the rough surface and remove local spikes by smoothening surface imperfection and reducing R_{rms} values. Moreover, as shown in Fig. 5, conductive AFM analysis clearly demonstrates that the AgNWs/HAT-CN (150 nm) film shows very uniform conductivity because current can not only be measured at AgNWs but also in the empty spaces between AgNWs. Therefore, all the PHOLEDs can operate properly without any electrical shorts. These results imply that employing a thick HAT-CN layer over 150 nm can give rise to reliable PHOLEDs, leading to an increase of the fabrication yield. It is well-known that lowering of the charge injection barrier enables improvement of the device's efficiency. For organic molecules adsorbed on metal electrodes, charge injection barriers intensely depend on the effective work function of the organic molecules-metal interface.[31] To understand the hole injection mechanism from AgNWs TCE to HAT-CN HIL, we examined the effective work function of Ag TCE – HAT-CN interface using an ultraviolet photoelectron spectroscopy (UPS) as shown in Fig. 6a.

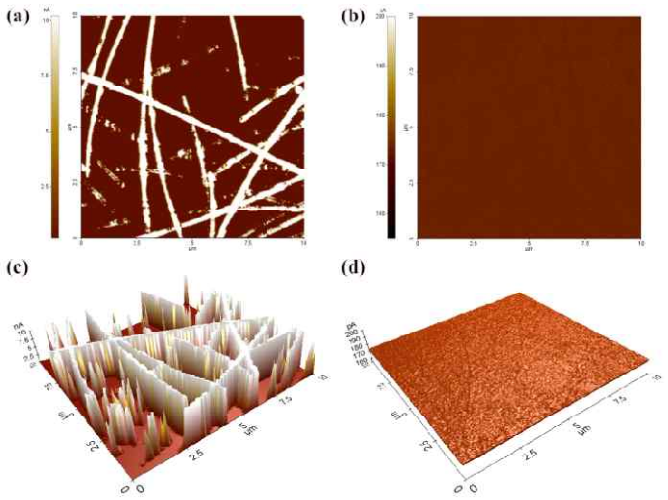

Fig. 5 Conductive AFM topographies of AgNWs and AgNWs/HAT-CN (150 nm) films on glass substrates : 2D images of (a) AgNWs and (b) AgNWs/HAT-CN, 3D images of (c) AgNWs and (d) AgNWs/HAT-CN.

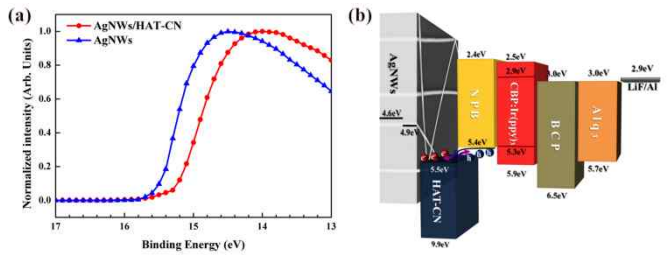

Fig. 6 Characterization of effective work function of Ag TCE – HAT-CN interface. (a) UPS spectra of AgNWs TCE and AgNWs TCE/HAT-CN films. (b) Energy band diagram of a PHOLED with AgNWs TCE and HAT-CN HIL.

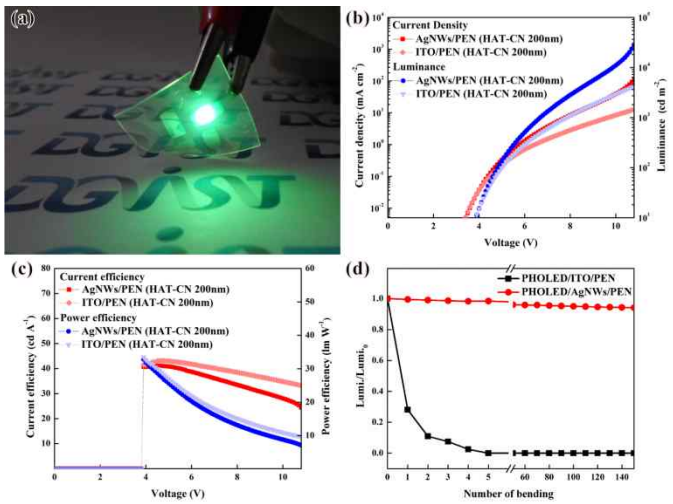

Fig. 7 Device performance of a flexible PHOLED with AgNWs TCE and HAT-CN HIL. (a) A picture of a flexible PHOLED with AgNWs/PEN TCE and HAT-CN HIL. (b) Current density-voltage-luminance (J-V-L) characteristics and (c) current and power efficiencies of a flexible PHOLED with AgNWs/PEN TCE and HAT-CN HIL. (d) Mechanical flexibility test of the PHOLEDs with AgNWs/PEN and ITO/PEN TCEs.

We prepared AgNWs and AgNWs/HAT-CN TCEs for UPS measurements. The AgNWs/HAT-CN TCE was prepared by thermal evaporation of HAT-CN onto a AgNW film in a high vacuum thermal evaporator. The film thickness of HAT-CN on the AgNWs TCE was 1.2 nm. The work function was measured from secondary electron cutoff in UPS spectrum. It was found that the work function of the AgNWs TCE increased from 4.6 eV to 4.9 eV drastically when HAT-CN was adsorbed onto the AgNWs TCE. This result clearly indicates that the work function of the AgNWs TCE can be changed by pre-covering the AgNWs surface with HAT-CN molecules in the monolayer regime. Recently, P. Amsalem et. al. reported that HAT-CN molecules form a regular honeycomb structure on Ag surface and strongly interact with the Ag surface and can diffuse into the Ag surface, leading to an increase of work function of the Ag electrode and a decrease of the hole injection barrier from Ag electrode to HAT-CN.[32] Furthermore, the LUMO energy level of HAT-CN molecules becomes Fermi-level pinned, resulting in an additional increase of work function of Ag electrode.[33] This is a good agreement with our observation in work function change of the AgNWs TCE caused by HAT-CN HIL. Therefore, the increased work function of the AgNWs TCE can induce the energy level alignment (ELA) between HAT-CN and AgNWs TCE, leading to a decrease of the hole injection barrier. Furthermore, The LUMO energy level of HAT-CN (-5.5 eV) is very close to the HOMO energy level of α-NPB (-5.4 eV), resulting in low energy offset. This low energy offset enables the electrons from the HOMO energy level of α-NPB to easily excite to the LUMO energy level of HAT-CN, leading to separation of holes and electrons by charge generation phenomenon.[34] This phenomenon results in the LUMO energy level pinning of HAT-CN molecules located at the interface with the α-NPB. Therefore, an efficient charge transport pathway can be achieved between the HAT-CN and α-NPB (Fig. 6b). As a result, incorporating a thick HAT-CN film as a HIL can improve device performances of OLEDs significantly. We also fabricated flexible PHOLEDs with the patterned AgNWs and ITO TCEs on a 2.5 x 2.5 cm^2 polyethylene naphthalate (PEN) film as shown in Fig. 7a. To fabricate reliable and flexible PHOLEDs, 200 nm thick HAT-CN layer was deposited onto the patterned AgNWs or ITO/PEN TCE. As shown in Fig. 7b and c, the current density − voltage − luminance (J − V − L) characteristics of flexible PHOLEDs exhibited similar device performances as fabricated PHOLEDs on glass substrates.

In addition, the device characteristics of flexible PHOLEDs with AgNWs/PEN TCE were almost similar to those of the ITO/PEN TCE based PHOLEDs (Table S2). As for the flexible PHOLED with AgNWs TCE, the turn-on voltage was only 3.9 V. It is noteworthy that the flexible PHOLEDs achieved high luminance over 60,000 cdm^{-2}. The maximum current and power efficiencies were 41.1 cdA^{-1} and 32.8 lmW^{-1}, implying that extremely flexible and high-performance PHOLEDs can be fabricated by using the AgNWs TCE and HAT-CN HIL. In order to compare the mechanical flexibility of the PHOLEDs with AgNWs/PEN and ITO/PEN TCEs, the device performance was measured as a function of wrapping cycles as shown in Fig. 7d. In this test, the device operation voltage and initial luminous intensity of a PHOLED with the AgNWs/PEN or ITO/PEN TCEs were 6V and 500 cd/m^2. Then, each PHOLED was rolled around bending radius of 7.5 mm, subsequently unrolled. The luminous intensity of each PHOLED was compared to its initial value. Within the first few cycle of this process, the PHOLEDs with ITO/PEN TCE began to partially emit a light and lost the luminous intensity sharply, resulting in electrical open circuits. Since ITO is an inorganic material, it is inherently brittle and cracks when exposed to a minimal amount of strain. Thus, cracks of ITO TCE can increase the sheet resistance of the anode or disrupt the OLEDs (Fig. S6 and Movie S2). On the other hand, the luminous intensity of the PHOLED with AgNWs/PEN TCE remained almost unchanged even after more than 150 wrapping cycles, verifying that the PHOLEDs with AgNWs/PEN TCE possesses an excellent mechanical flexibility (Movie S3).

In conclusion, we successfully fabricated extremely flexible and high-performance PHOLEDs with AgNWs TCE and n-type HAT-CN HIL. The fabricated PHOLEDs exhibited excellent device characteristics such as very low turn-on voltage (3.6 V) and extremely high current and power efficiencies (44.5 cdA^{-1} and

35.8 lmW^{-1}). In addition, flexible PHOLEDs with the AgNWs TCE and HAT-CN HIL fabricated onto plastic substrates showed remarkable mechanical flexibility as well as device performance. We found that employing a thick HAT-CN film as a HIL between AgNWs TCE and α-NPB could decrease the hole injection barrier, leading to significant improvement in current and power efficiencies of the PHOLEDs. Furthermore, the fabrication yield of PHOLEDs was greatly increased by introducing a thicker HAT-CN layer on the AgNWs TCE without any loss of efficiency. Further improvement in device performance can be expected if the material and device structure can be further optimized. We anticipate that the AgNWs TCE in combination with HAT-CN HIL can be a promising platform for realization of flexible and high performance OLEDs which are next-generation displays.

Acknowledgements

This research was supported by Basic Science Research Program through the National Research Foundation of Korea (NRF) funded by the Ministry of Education, Science, and Technology (2012R1A1A1040811). This work was also supported by the DGIST MIREBraiN Program and DGIST R&D Program of Ministry of Education, Science, and Technology of Korea (14-BD-0404). This work was supported by the 2014 Research Fund of UNIST(Ulsan National Institute of Science and Technology).

Notes and references

[a] Department of Energy Systems Engineering, Daegu Gyeongbuk Institute of Science and Technology (DGIST), 50-1 Sang-Ri, Hyeonpung-Myeon, Dalseong-Gun, Daegu, 711-873, Korea.

[b] Display Nanomaterials Institute (DNI), Kyungpook National University, 1370 Sankyuk-Dong, Buk-Ku, Daegu, 702-701, Korea.

[c] Department of Materials Science and Engineering, Ulsan National Institute of Science and Technology (UNIST), UNIST-gil 50, Ulsan, 689-798, Korea.

† Electronic Supplementary Information (ESI) available: The preparation and characterization of AgNWs TCE with various conditions, SEM images and AFM topographies of HAT-CN films with different thickness on the AgNWs TCE, mechanical flexibility test of flexible PHOLEDs with ITO/PEN and AgNWs/PEN TCEs, and detailed information about materials are included. See DOI: 10.1039/c000000x/

1 C. Murawski, K. Leo and M. C. Gather, *Adv. Mater.*, 2013, **25**, 6801-6827.

2 W. Gaynor, S. Hofmann, M. G. Christoforo, C. Sachse, S. Mehra, A. Salleo, M. D. McGehee, M. C. Gather, B. Lüssem, L. Müller-Meskamp, P. Peumans and K. Leo, *Adv. Mater.*, 2013, **25**, 4006-4013.

3 J. Liang, L. Li, X. Niu, Z. Yu and Q. Pei, *Nat. Photon.*, 2013, **7**, 817-824.

4 S. R. Forrest, *Nature*, 2004, **428**, 911-918.

5 H. Han, D. Adams, J. W. Mayer and T. L. Alford, *J. Appl. Phys.*, 2005, **98**, 083705.

6 Y. Sun, N. C. Giebink, H. Kanno, B. Ma, M. E. Thompson and S. R. Forrest, *Nature*, 2006, **440**, 908-912.

7 S. Chen, L. Deng, J. Xie, L. Peng, L. Xie, Q. Fan and W. Huang, *Adv. Mater.*, 2010, **22**, 5227-5239.

8 Z. B. Wang, M. G. Helander, J. Qiu, D. P. Puzzo, M. T. Greiner, Z. M. Hudson, S. Wang, Z. W. Liu and Z. H. Lu, *Nat. Photon.*, 2011, **5**, 753-757.

9 J. Kido, M. Kimura and K. Nagai, *Science*, 1995, **267**, 1332-1334.

10 L. Xiao, Z. Chen, B. Qu, J. Luo, S. Kong, Q. Gong and J. Kido, *Adv. Mater.*, 2011, **23**, 926-952.

11 C. W. Lee and J. Y. Lee, *Adv. Mater.*, 2013, **25**, 5450-5454.

12 A. Kumar and C. Zhou, *ACS Nano*, 2010, **4**, 11-14.

13 O. Inganäs, *Nat. Photon.*, 2011, **5**, 201-202.

14 Z. Yu, L. Li, Q. Zhang, W. Hu and Q. Pei, *Adv. Mater.*, 2011, **23**, 4453-4457.

15 Z. Yu, Q. Zhang, L. Li, Q. Chen, X. Niu, J. Liu and Q. Pei, *Adv. Mater.*, 2011, **23**, 664-668.

16 L. Li, Z. Yu, W. Hu, C. h. Chang, Q. Chen and Q. Pei, *Adv. Mater.*, 2011, **23**, 5563-5567.

17 W. Gaynor, G. F. Burkhard, M. D. McGehee and P. Peumans, *Adv. Mater.*, 2011, **23**, 2905-2910.

18 R. Zhu, C.-H. Chung, K. C. Cha, W. Yang, Y. B. Zheng, H. Zhou, T.-B. Song, C.-C. Chen, P. S. Weiss, G. Li and Y. Yang, *ACS Nano*, 2011, **5**, 9877-9882.

19 D. -S. Leem, A. Edwards, M. Faist, J. Nelson, D. D. C. Bradley and J. C. de Mello, *Adv. Mater.*, 2011, **23**, 4371-4375.

20 D. Lee, H. Lee, Y. Ahn, Y. Jeong, D.-Y. Lee and Y. Lee, *Nanoscale*, 2013, **5**, 7750-7755.

21 D. Y. Choi, H. W. Kang, H. J. Sung and S. S. Kim, *Nanoscale*, 2013, **5**, 977-983.

22 Y. Ahn, Y. Jeong and Y. Lee, *ACS Appl. Mater. Interfaces*, 2012, **4**, 6410-6414.

23 J.-Y. Lee, S. T. Connor, Y. Cui and P. Peumans, *Nano Lett.*, 2008, **8**, 689-692.

24 P. Lee, J. Lee, H. Lee, J. Yeo, S. Hong, K. H. Nam, D. Lee, S. S. Lee and S. H. Ko, *Adv. Mater.*, 2012, **24**, 3326-3332.

25 J. Lee, P. Lee, H. Lee, D. Lee, S. S. Lee and S. H. Ko, *Nanoscale*, 2012, **4**, 6408-6414.

26 L. Li, Z. Yu, C.-h. Chang, W. Hu, X. Niu, Q. Chen and Q. Pei, *Phys. Chem. Chem. Phys.*, 2012, **14**, 14249-14254.

27 B. S. Mashford, M. Stevenson, Z. Popovic, C. Hamilton, Z. Zhou, C. Breen, J. Steckel, V. Bulovic, M. Bawendi, S. Coe-Sullivan and P. T. Kazlas, *Nat. Photon.*, 2013, **7**, 407-412.

28 H. Sasabe, H. Nakanishi, Y. Watanabe, S. Yano, M. Hirasawa, Y. J. Pu and J. Kido, *Adv. Funct. Mater.*, 2013, **23**, 5550-5555.

29 W. S. Jeon, J. S. Park, L. Li, D. C. Lim, Y. H. Son, M. C. Suh and J. H. Kwon, *Org. Electron.*, 2012, **13**, 939-944.

30 S. H. Cho, S. W. Pyo and M. C. Suh, *Synth. Met.*, 2012, **162**, 402-405.

31 H. Ishii, K. Sugiyama, E. Ito and K. Seki, *Adv. Mater.*, 1999, **11**, 605-625.

32 P. Amsalem, A. Wilke, J. Frisch, J. Niederhausen, A. Vollmer, R. Rieger, K. Müllen, J. P. Rabe and N. Koch, *J. Appl. Phys.*, 2011, **110**, 113709.

33 H. Glowatzki, B. Bröker, R.-P. Blum, O. T. Hofmann, A. Vollmer, R. Rieger, K. Müllen, E. Zojer, J. P. Rabe and N. Koch, *Nano lett.*, 2008, **8**, 3825-3829.

34 Y.-K. Kim, J. W. Kim and Y. Park, *Appl. Phys. Lett.*, 2009, **94**, 063305.

